Chemical Engineering Journal xxx (xxxx) xxx–xxx

Contents lists available at ScienceDirect

Chemical Engineering Journal

journal homepage: www.elsevier.com/locate/cej

Non-oxidative methane conversion in microwave-assisted structured reactors

Ignacio Julian[a], Heidy Ramirez[a], Jose L. Hueso[a,b], Reyes Mallada[a,b,*], Jesus Santamaria[a,b]

[a] Institute of Nanoscience of Aragon (INA) and Department of Chemical and Environmental Engineering, University of Zaragoza, Campus Rio Ebro, I+D+i Building, 50018 Zaragoza, Spain

[b] Networking Research Center on Bioengineering, Biomaterials and Nanomedicine (CIBER-BBN), 28029 Madrid, Spain

HIGHLIGHTS

- Mo-ZSM5@SiC Structured catalytic reactor stable operation under MW heating at reaction conditions.
- Acetylene formation in the MNOC reaction under MW heating.
- Product distribution under MW heating is different than in the case of conventional heating.
- Gas-solid temperature gap prevents soft-coke formation.

ARTICLE INFO

Keywords:
Microwave-assisted heterogeneous catalysis
Methane non-oxidative coupling
Methane dehydroaromatization
Gas-solid temperature gradient
Microwave selective heating
MoZSM5

ABSTRACT

The main problem to be addressed in the valorization of methane under non-oxidative conditions (MNOC) is to reduce or even avoid coke formation. In this work we report the use of microwave-assisted heating for MNOC. We have developed a system able to heat-up a Mo-ZSM5 catalyst coated on silicon carbide monolith that could operate stable for at least 19 h at reaction conditions, 700 °C. We demonstrate that under MW-heating the selectivity shifts to C_2s and benzene. In contrast, the operation under conventional heating (CH) produces more coke and polyaromatics. The selective microwave heating has two effects in this reaction: i) during the activation of the catalyst the formation of the active catalytic species of Mo_2C inside the microporous support is different affecting the selectivity and product distribution; ii) a gas-solid temperature gradient is established that prevents the formation of coke from PAHs in the gas phase. The MNOC process under controlled MW heating at high space velocity (3000 mL/g_{cat}·h) gives a hydrocarbon yield of around 6% with a very low deactivation rate. These results open up new possibilities for process intensification using alternative sources of energy, as is the case of microwaves, for heating structured catalytic reactors.

1. Introduction

Natural gas is one of the main current energy alternatives, given the large number of existing reserves (193.5 Tm^3 in 2017 [1]). However, despite its availability and abundance, the use of methane as raw material is still limited due to transportation costs and the absence of efficient direct methane transformation routes into valuable chemicals which can compete with the oil based production of chemicals [2].

Main challenges in the direct methane non-oxidative coupling (MNOC) process are thermodynamic limitations that constrain methane conversion at low temperature and the inherent coke deposition over the active sites of the employed catalysts leading to fast deactivation. Among the direct MNOC routes, methane dehydroaromatization (MDA) is a well-established endothermic process to produce aromatics (mainly benzene and naphthalene) as well as C_2 species (ethylene) in the presence of Mo/ZSM-5 (e.g. [3,4]) or Mo/MCM-22 [5–8] based catalysts. Typical methane dehydroaromatization conversions are 10–15% with selectivity to aromatics in the range 60–90% working at 700 °C under conventional heating, using spatial velocities in the range 1400–1600 mL/g_{cat}·h and being the optimal molybdenum load in the range 3–6% wt [9–14].

Although the mechanism of the Mo-containing zeolites has not been resolved yet [15], it is widely accepted that the MDA reaction mechanism is initiated via the formation of methyl radicals on Mo_2C active

* Corresponding author at: Institute of Nanoscience of Aragon (INA) and Department of Chemical and Environmental Engineering, University of Zaragoza, Campus Rio Ebro, I+D+i Building, 50018 Zaragoza, Spain.
E-mail address: rmallada@unizar.es (R. Mallada).

https://doi.org/10.1016/j.cej.2018.08.150

sites followed by a series of parallel and consecutive reactions that end up with the formation of benzene and naphthalene within the zeolite channels [10,16–19] due to the shape-induced selectivity of their micropores (0.51–0.56 nm) [2,20,21]. The reaction continues out of the pores leading to methyl aromatics (toluene, xylenes, etc.), polyaromatics and highly dehydrogenated carbon species, i.e. coke. Among coke sources, the graphitic-like carbon deposits are associated to molybdenum on the active sites and the carbidic carbon in molybdenum carbide (Mo_2C) or Mo-oxycarbide (MoO_xC_y) [22-26]. Although both coke types contribute to catalyst deactivation, the selectivity loss is mainly attributed to the soft coke, i.e. zeolite pore blocking, and the activity loss may be better explained with the hard coke on the Mo_2C active sites.

The actual strategies devoted to minimize coke deposits on the active sites focus on the improvement of metal dispersion [15,27–29]. The better the Mo dispersion, the lower clustering and coking probability. Additionally, the co-generation of unwanted byproducts such as soft coke or heavy polyaromatics derived from gas-phase reactions may be partially inhibited tuning the contact time [5,30]. Nevertheless, this parameter is somehow constrained as it must be strongly linked to the intrinsic reaction kinetics and diffusion mechanisms in order to optimize the production rate of the desired products, i.e. ethylene, benzene, etc.

In this work, we propose the use of microwave energy to tackle the two causes of coke formation discussed above. The use of microwave reactors is an ideal way to increase the energy efficiency of this process since the heat demanded to drive this endothermic reaction can be directly supplied to the catalyst, either by absorbing microwave radiation by itself or by deploying it on a microwave susceptor material [31–33]. With respect to conventional heating mechanisms involving conduction, convection and radiation, microwave heating provides fast and direct heating of the target materials, including the active phases. The selective heating would have an effect on the carburization process during the formation of the active Mo_2C phase [34,35]. On the other hand, microwave heating may generate a solid-gas temperature gradient that can become advantageous for the process in terms of inhibition or minimization of undesired gas-phase reactions [34,36].

The microwave heating mechanism in solids is often complex and varies depending on the solid nature [37–39]. Nevertheless, the heating principle can always be described in terms of the dielectric properties of the material: dielectric constant (ε'), dielectric loss (ε'') and the loss tangent (δ), which is the ratio of ε'' and ε' [34,35,40]. The dielectric constant (ε') represents the ability of the material to be polarized by an electrical field (i.e. store energy from an electrical field) while the dielectric loss (ε'') refers to the capacity of the material to dissipate the radiation in the form of heat. Thus, a material with high loss tangent (δ) is always desirable for efficient MW heating.

In the present study, two main topics concerning MW-assisted heterogeneous catalysis in the MNOC process have been addressed: (i) Evaluation of different heating-target monolithic supports. The benchmark MNOC catalyst Mo/ZSM-5 (4% wt. Mo, SiO_2/Al_2O_3 = 23) has been coated both on cordierite (nearly MW-transparent material) and on SiC-β (excellent MW-absorber) monoliths in order to compare the heating controllability and process performance of the MW-assisted MNOC reaction. Structured catalyst configurations allowed minimizing pressure drop and mass-transfer limitations and facilitated the desorption of targeted-products in a comparative cooler gas stream with respect to a fixed-bed configuration; (ii) Evaluation of the effect of the heating mode (either conventional or MW irradiation) on the methane conversion and hydrocarbon products selectivity for the above mentioned structured catalyst subjected to the non-oxidative methane coupling reaction at 700 °C working at spatial velocities ranging from 3000 to 6000 mL/g_{cat}·h. The purpose of using high spatial velocities with respect to those reported in literature for this reaction is twofold: a) to shorten gas-solid contact time in order to minimize coke production and to look for reaction intermediates under each heating mode; b) to evaluate the MNOC process efficiency using higher and more attractive methane throughputs.

2. Experimental

2.1. Preparation of the catalytic monoliths

An incipient wetness impregnation method was employed to incorporate the molybdenum precursor into the parent H-ZSM-5 zeolite (Zeolyst CBV2314, SiO_2/Al_2O_3 = 23). The required amount of ammonium heptamolybdate, $(NH_4)_6Mo_7O_{24}{\cdot}4H_2O$ (*Sigma Aldrich*), to obtain 4% wt. Mo on the catalyst, was dissolved in deionized water and poured drop wise into the zeolite under continuous mixing until incipient wetness was achieved. The impregnation was followed by drying at 120 °C and calcination in air (heating ramp: 1 °C/min) at 550 °C during 6 h following the procedure described by Wang et al. 1997 [4].

Two types of structured monoliths were employed, cordierite ceramic ($2MgO\ 2Al_2O_3\ 5SiO_2$, *Corning*) and silicon carbide (SiC-β, *SICAT*), being their cell density 400 and 200 cpsi, respectively. The parent monoliths were cut down into small cylindrically-shaped samples of 15 mm height and 9 mm diameter to be tested in the monomodal MW resonator. This specific monolith size was selected to overlap with the maximum electromagnetic field generated within the MW cavity. Prior to the washcoating process, the outer surfaces of the monoliths were covered with Teflon tape to avoid coating on the external walls.

The Mo/ZSM-5 catalyst was deposited on the surface of the monoliths following a conventional wash-coating method. This process involved the following steps: a) monolith immersion in the slurry solution containing the desired material, b) monolith withdrawal at constant speed, c) removal of the slurry excess from the channels, d) solvent evaporation and e) calcination (Fig. 1.a). Steps a) to d) were repeated to get the desired catalytic load. The quality of the final coating depended mainly on the slurry properties, withdrawal speed and the technique used to remove the slurry excess.

The reagents used to prepare the slurry were deionized water, PVA (Polyvinyl alcohol 85000–124000 MW, *Sigma Aldrich*) as binder, colloidal silica (*LUDOX AS-30*, *Sigma Aldrich*) to increase the viscosity of the slurry and improve the adherence to the support and the zeolite-based catalytic powder (4% wt. Mo/ZSM-5). The following molar composition was employed, (H_2O: PVA: SiO_2: Mo/ZSM-5) = (61: 3: 6: 30), according to a previous protocol reported by Eleta et al. 2009 [41]. The viscosity of the resulting slurry, measured using a rotational rheometer Visco Basic Plus (*Fungilab*) was 0.17 Pa·s at lab temperature. The wash-coating process was carried out using a commercial dip-coater *KSV Nima* (KN4001) which controls the withdrawal speed. An axial velocity of 10 mm/min was employed for all coating tests. The coating process was followed by the injection of compressed air through the monolith channels in order to drag the slurry excess. An air blowing gun was used for this purpose. The coated sample was then heated to 90 °C in order to evaporate the remaining solvent traces. The fourth and last coating cycle finalized with a calcination step at 550 °C (1 °C/min) during 6 h. Fig. 1.b shows a detail of uncoated and coated SiC monolith with a Mo/ZSM-5 catalytic layer. The experiments have been performed by the platform of Production of Biomaterials and Nanoparticles of the NANBIOSIS ICTS, more specifically by the Nanoparticle Synthesis Unit of the CIBER in BioEngineering, Biomaterials & Nanomedicine (CIBER-BBN).

2.2. Characterization of the structured catalysts

Raman spectroscopy measurements were performed to identify the presence and coordination of Mo species in the catalytic samples. An Alpha 300 Raman spectrometer from WITec with 532 nm laser source and CCD camera as detector were employed on purpose. The selected laser power and integration time were 8 mW and 2 s, respectively. Argon adsorption was employed to study the textural properties of the

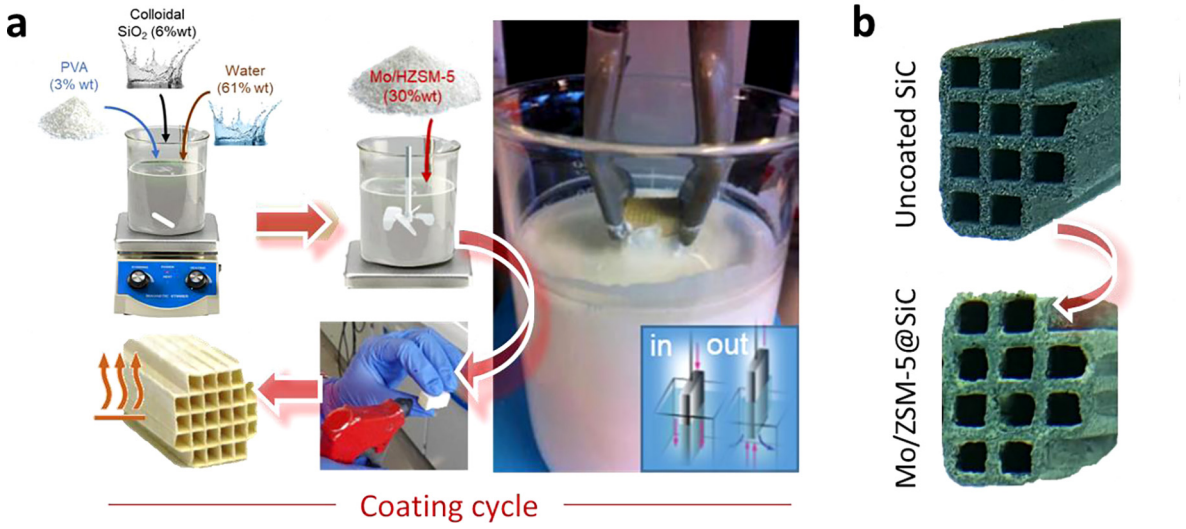

Fig. 1. a) Scheme depicting the different steps implied in the progressive coating cycle of the monoliths with a slurry containing the Mo/ZSM-5 catalyst; b) digital photograph comparing an uncoated and coated SiC monolith with Mo/ZSM-5 catalytic layer, respectively.

catalysts, evaluating the adsorption isotherm. The specific surface area was calculated by BET equation, considering consistency criteria proposed by Rouquerol for microporous materials [42] and the micropore volume was evaluated at $P/P_0 = 0.01$. The measurements were carried out using a Micromeritics ASAP 2020 analyzer. Samples were degassed at 350 °C prior to the analysis. Transmission Electron Microscopy TEM (Tecnai F30, *FEI*) and Scanning-TEM (Titan Low Base 60–300, *FEI*) were employed to visualize the catalyst structure in detail and to evaluate the dispersion of Mo species and the eventual formation of aggregates on the zeolite external surface. SEM-EDX was used to study the morphology of the catalysts and Mo distribution on the surface of the zeolite support as well as to measure the thickness of the catalyst coating on the monolith. The analyses were carried out in a scanning electron microscope INSPECT-F50 from *FEI* Company.

Additionally, the evolution of the dielectric properties (dielectric constant, ε', and dielectric loss, ε'') with temperature of the different involved materials, i.e. HZSM-5, Mo/ZSM-5 and SiC-β powders, were measured by the Microwave Division (DIMAS) group of the research institute ITACA at the Polytechnical University of Valencia, UPV (Spain) and evaluated from 20 to 850 °C, in a dual mode cylindrical cavity following the methodologies previously described [43].

2.3. Experimental set-up

The synthesized catalysts were tested for methane non-oxidative coupling under conventional and microwave-assisted heating. The experimental set-up is depicted in Fig. 2.a. Three mass flow controllers (Bronkhorst 0–20 mLSTP/min) were employed to feed the reactive mixture (CH_4:N_2 = 80:20 or 75:25) or catalyst regeneration flow (N_2:O_2 = 19:1) into the reactor which consist of a quartz tube (12 mm external diameter) loaded with the structured Mo/ZSM-5@SiC or Mo/ZSM-5@cordierite catalyst. The catalyst was heated under reaction atmosphere up to the reaction temperature 700 °C, using a heating ramp of 20 °C/min. The selected spatial velocity for the catalytic tests was varied between 3000 and 6000 mL_{STP}/g_{cat}·h.

The reactor was placed either within an electrical oven or within a monomodal microwave resonator prototype designed and fabricated by the DIMAS group (Polytechnical University of Valencia, Spain). The inner cylindrical resonator dimensions are 104.92 mm diameter and 85 mm height. The microwave cavity operates in the TE_{111} single mode around the resonant frequency of 2.45 GHz exhibiting a strong and uniform electric field where the test sample is positioned, i.e. the center of the resonator, as described by Catalá-Civera et al. 2015 [43]. The theoretical resonant frequency of the TE_{111} mode is 2.432 GHz, as calculated by analytical expressions [44].

Fig. 2.b shows a detail of the microwave resonator including the set of contactless thermometers, the digital camera and the reactor. The temperature of the sample was measured by an infrared camera (*Optris PI 1 M*) and a pyrometer (*Optris CTlaser LT*) pointing at the sample through 8 mm holes drilled in the resonator. The relative position of each non-contact thermometer with respect to the sample and the microwaves inlet port is illustrated in Fig. 2.b. The pyrometer works in a temperature range from −50 °C to 975 °C using a spectral range of 8–14 μm and is not able to measure through quartz. In contrast, the *PI 1 M* camera (450 °C −1800 °C) enables this measurement since it works in a 0.92–1.1 μm spectral range that does not interfere with quartz transmission. Temperature corrections were applied in order to estimate the sample temperature as a function of quartz wall temperature measured with the pyrometer. The resonator prototype incorporates PID control software that tuned the MW frequency bandwidth (0.05–100 MHz) at a given input power (110 W), in order to control the sample heating rate and temperature, measured with the IR pyrometer. In the case of conventional heating, CH, the sample temperature in the electrical oven was measured and controlled with a thermocouple placed within the central monolith channel.

The outlet reaction gases were conducted through a heated pipe (230 °C) into a gas chromatograph (*Thermo Fisher Trace 1300* with auxilliary oven *Trace 1310*) in which 4 different columns and 3 detectors allow the identification and quantification of permanent gases (TCD), light hydrocarbons (FID1) and aromatics (FID2) in less than 10 min of analysis. Methane conversion (x_{CH4}) and hydrocarbon selectivity (S_{CxHy}) were calculated using Equations (1) and (2), being $\dot{n}_i$, $\dot{V}_i$, A_i and RF_i the molar flow, volumetric flow, peak area and response factor of the species *i*, respectively. The response factor is the ratio between the response of a detector to a compound (peak area) and the concentration of that compound in a mixture of gases. The hydrocarbon yield (Y_{CxHy}) is defined as the product of conversion by selectivity.

$$x_{CH_4} = \frac{\dot{n}_{CH_4,in} - \dot{n}_{CH_4,out}}{\dot{n}_{CH_4,in}} = \frac{\dot{V}_{CH_4,in} - \frac{A_{CH_4,out}/RF_{CH_4}}{A_{N_2,out}/RF_{N_2}}\dot{V}_{N_2,in}}{\dot{V}_{CH_4,in}} \quad (1)$$

$$S_{C_xH_y} = x\hat{A}\cdot\frac{\dot{n}_{C_xH_y,out}}{\dot{n}_{CH_4,in} - \dot{n}_{CH_4,out}} = x\hat{A}\cdot\frac{\frac{A_{C_xH_y,out}/RF_{C_xH_y}}{A_{N_2,out}/RF_{N_2}}\dot{V}_{N_2,in}}{\dot{V}_{CH_4,in} - \frac{A_{C_xH_y,out}/RF_{C_xH_y}}{A_{N_2,out}/RF_{N_2}}\dot{V}_{N_2,in}} \quad (2)$$

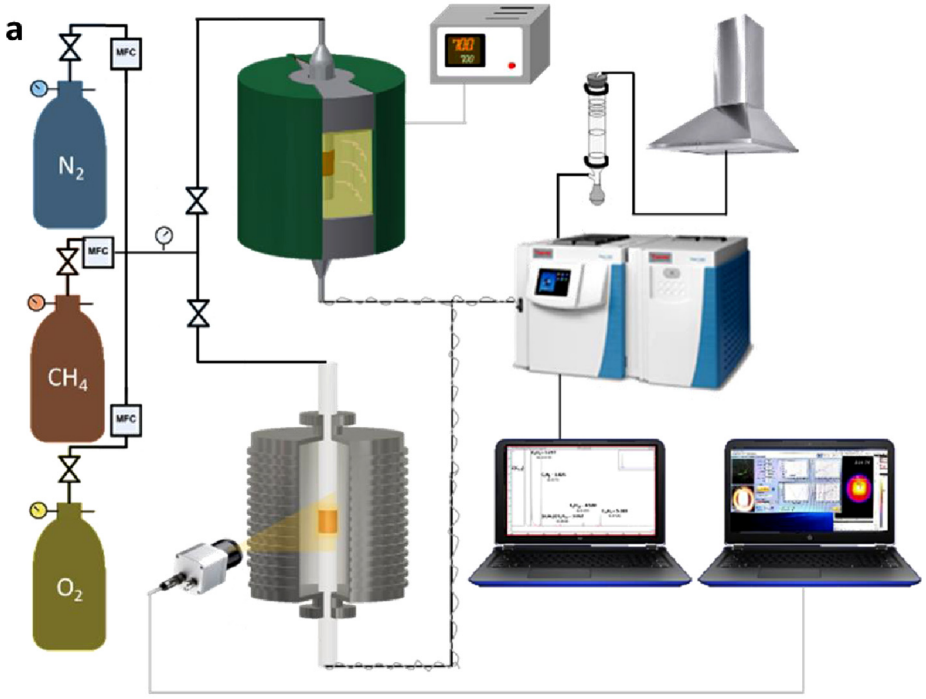

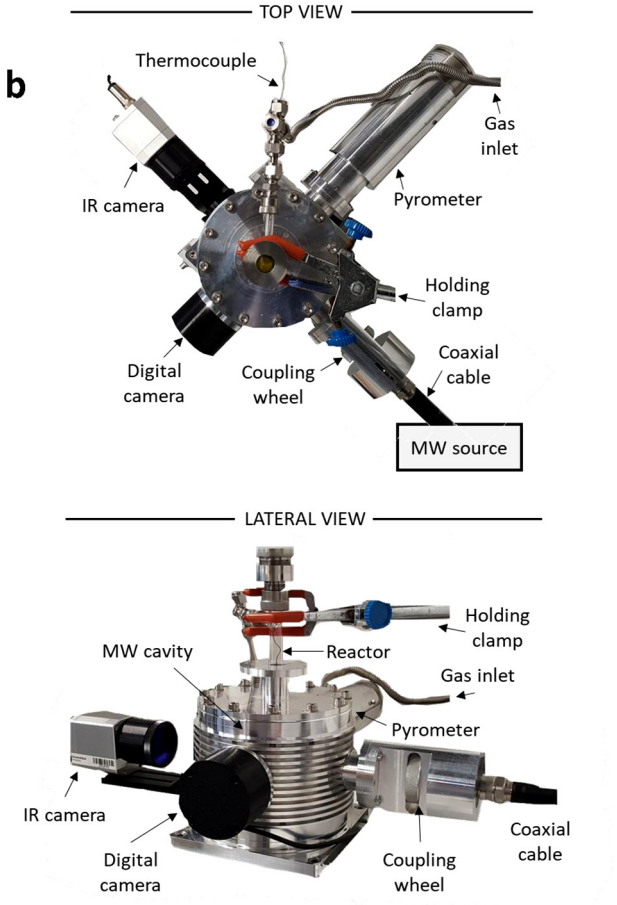

Fig. 2. a) Experimental set-up for methane non-oxidative coupling under conventional and microwave-assisted heating, b) top and lateral view of the employed MW resonator.

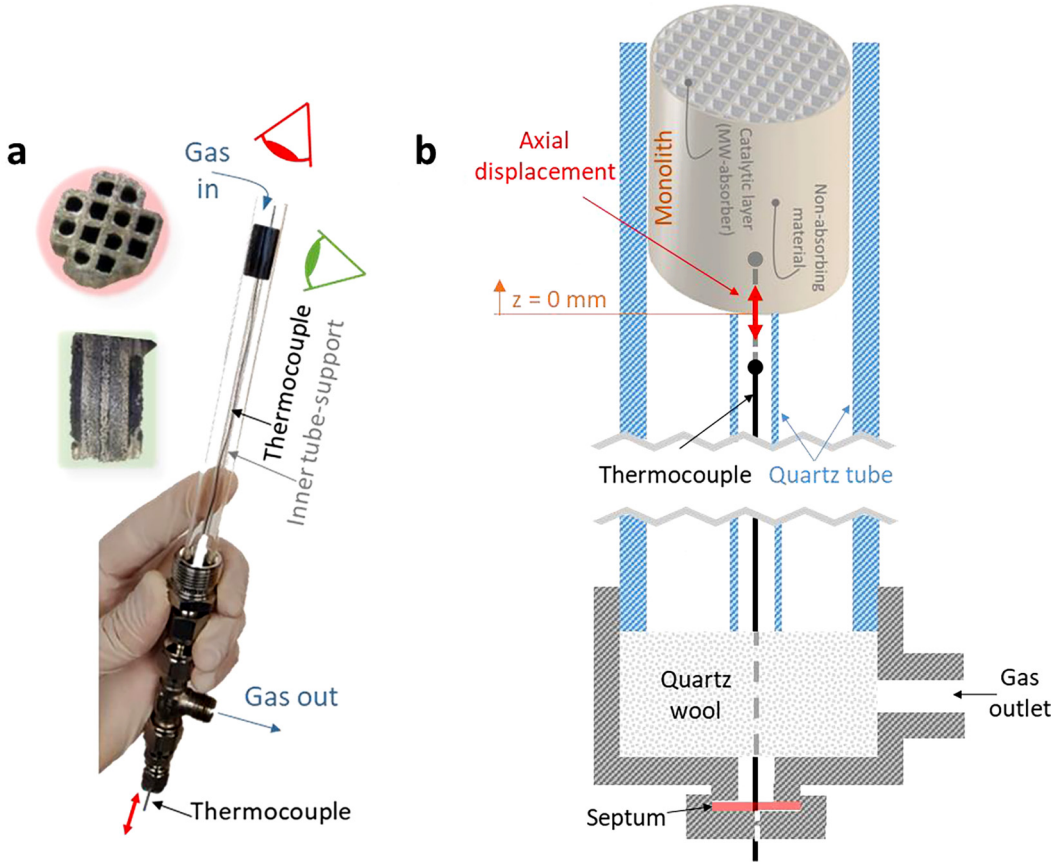

Fig. 3. a) Digital image of the reactor configuration for gas-solid temperature gradient measurement including top (red) and lateral (green) view of the structured catalyst, b) Reactor configuration scheme.

The calibration of the signal intensity of TCD and FID detectors with respect to the involved reaction gases was performed feeding to the GC several calibration gas mixtures containing a given concentration of the main reaction products: CH_4, CO, CO_2, C_2 species (ethane, ethylene and acetylene), C_3 species (propane, propylene and propadiene) and light aromatics (benzene and toluene), as well as the injection of solutions of known concentrations containing heavier aromatics (o,m,p-xylene and naphthalene), diluted in n-hexane. Calibration tests were performed using various dilutions of the employed gas mixtures in an inert gas (N_2) in order to quantify the response factor of each gas at different concentrations in the range of the production rates under MNOC. The linear trend between concentration and the peak area (TCD or FID output signal) for each gas at different concentrations allowed determining consistent RF_i values, which are valid along the evaluated concentration range for each species.

2.4. Gas phase temperature measurements

The gas phase temperature downstream was measured using the experimental reactor configuration depicted in Fig. 3. In both cases, MW and CH, a quartz sheath containing a moveable thermocouple (0.5 mm diameter) was located downstream the monolith. In the case of the microwave cavity this measurement was not straightforward since the thermocouple could interact with the electromagnetic (EM) field induced by the microwave source. In our case, thanks to the design of the cylindrical resonator [43] the maximum electromagnetic field is limited to a small region of the cavity (1.5 cm height, 1 cm diameter) and its intensity decays abruptly towards the cavity walls. Therefore, the thermocouple could be placed in-situ and be approached close enough (2 mm distance) to the heated sample under MW irradiation without disturbing and/or interfering with the electromagnetic field.

Additionally, the structured reactor configuration employed allowed us to confirm the existence of a gas-solid temperature gradient. In our previous work, we already measured the temperature gradient between gas and solid 'in situ', i.e. within the monolith channels, along a MW heating test under reactive atmosphere (ethylene epoxidation reaction). A gas-solid temperature gap of 40–50 °C was measured working at 200 °C in the solid phase [41]. In this work we used a simpler approach, which gave an estimation of the gas temperature at a certain point in the central part of the monolith. We turned off the MW power and quickly introduced the thermocouple through the sheath up to the central monolith channel.

Finally, the above mentioned system was employed for the validation of the temperature measurements given by the infrared camera and pyrometer, comparing the cooling curve, T(t), of both contactless thermometers and the thermocouple located at the centre of the sample, inserted immediately after switching off the microwave source.

3. Results and discussion

3.1. Catalyst and structured reactor characterization

The catalytic materials, both in powder form and coated on cordierite or SiC monoliths were characterized in order to evaluate their textural and chemical properties. A thorough characterization of the 4 wt% Mo/ZSM-5 powder is presented in Fig. 4. In order to gain further insight on the MoO_x structures formed at the impregnated sample, Raman spectroscopy (Fig. 4a) enabled to detect metal-oxide vibrational modes in the fresh catalyst. The absence of significant peaks at 300 cm^{-1} (Mo = O bending) [45], 678, 829 cm^{-1} (Mo-O-Mo stretching) and 1003 cm^{-1} (Mo = O stretching) [46] revealed that the sample does not contain MoO_3 crystallites or, at least, they are very well

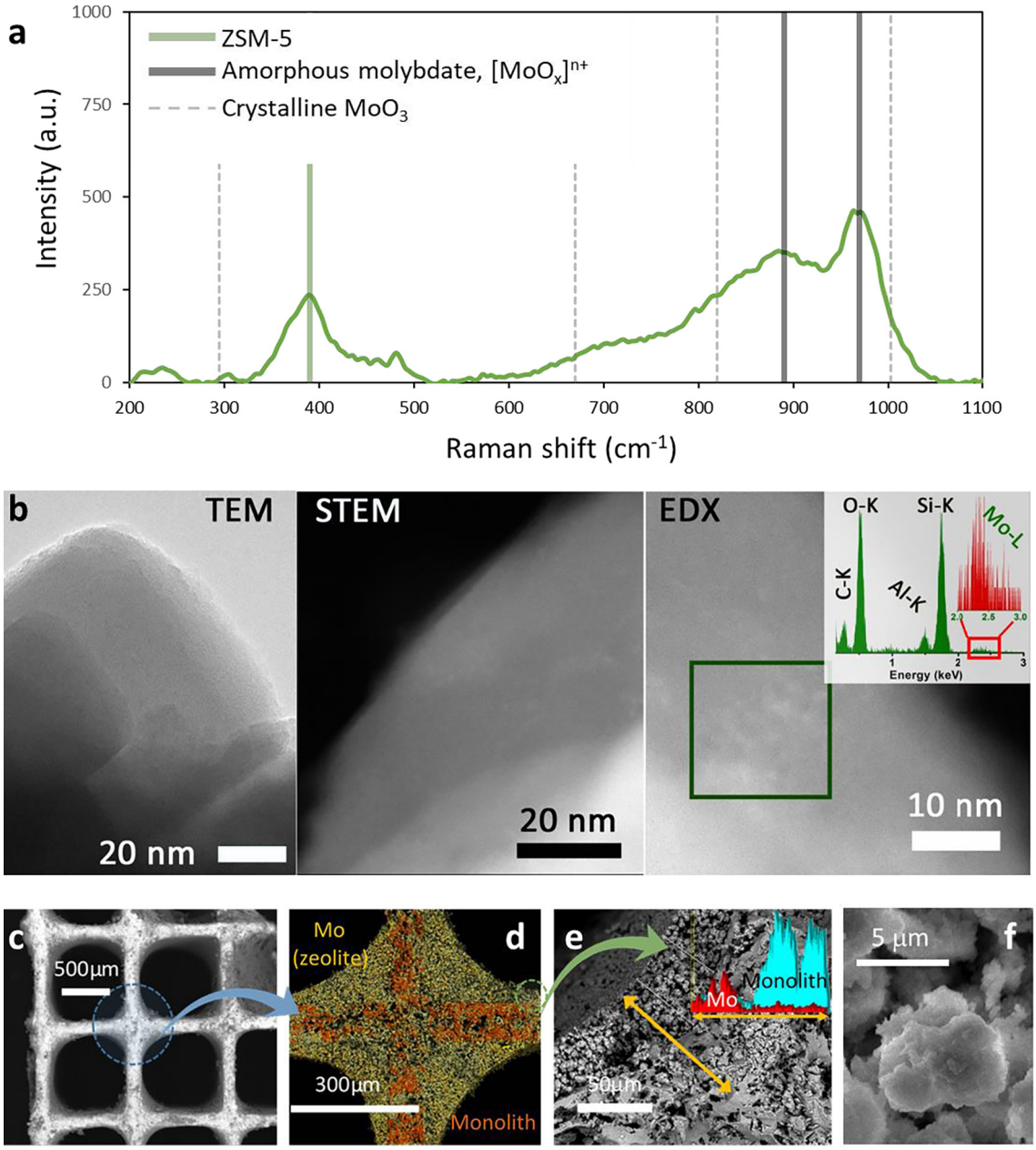

Fig. 4. a) Raman spectrum of Mo/ZSM-5 (4 wt%. Mo), b) TEM and STEM micrographs and EDX analysis, c) SEM micrograph of coated cordierite monolith, d) SEM-EDX mapping of Mo in yellow (Mo/ZSM-5) and Mg in orange (cordierite monolith), e) EDX signal of Mo and Mg along the selected line, f) SEM micrograph of Mo/ZSM-5 (4 wt%. Mo) powder.

dispersed along the zeolite channels. This was also corroborated by XRD (not shown) where no diffraction peaks corresponding to MoO_3 were detected. The broad band between 860 and 970 cm^{-1} observed in Fig. 4.a can be attributed to amorphous MoO_x. Actually, the peak at 970 cm^{-1} has been reported as the Mo = O stretching mode in exchanged MoO_x species within ZSM-5 channels, i.e. $(Mo_2O_5)^{2+}$ [45]. The band at 376 cm^{-1} corresponds to the lattice vibration of the zeolite.

The specific surface area 571 m^2/g and micropore volume 0.198 cm^3/g of the parent H-ZSM5 zeolite was reduced to 438 and 0.151 cm^3/g after the incorporation of Mo. The high Mo dispersion on the support in the fresh 4%Mo/ZSM-5 sample was confirmed by TEM and STEM due to the absence of Mo-based clusters or aggregates along the external zeolite surface (Fig. 4.b) that normally appear using higher metal loads. The EDX analysis confirms the incorporation of Mo inside the zeolitic pores.

Concerning the characterization of the catalyst coating on structured cordierite and SiC supports, the thickness and composition of the different coatings were evaluated by SEM-EDX. Fig. 4.c shows a SEM-EDX micrograph of a cordierite squared-cell monolith coated with Mo/ZSM-5. The use of squared cells led to catalyst accumulation on the channel corners and resulted in inhomogeneous coating of the structured support. This phenomenon, that was previously reported by some authors, e.g. [41,47], shall not affect the reaction performance under conventional heating but it may impact drastically the sample heating under MW irradiation, as it will be discussed later. The acquisition of EDX mappings of the structured catalysts allowed the identification of the different species in the sample. Fig. 4.d illustrates the distribution of Mo (from the catalyst) and Mg (from cordierite) species by means of EDX mapping. This enabled the determination of local and average coating thicknesses along the samples which is around 50 µm. The semi-

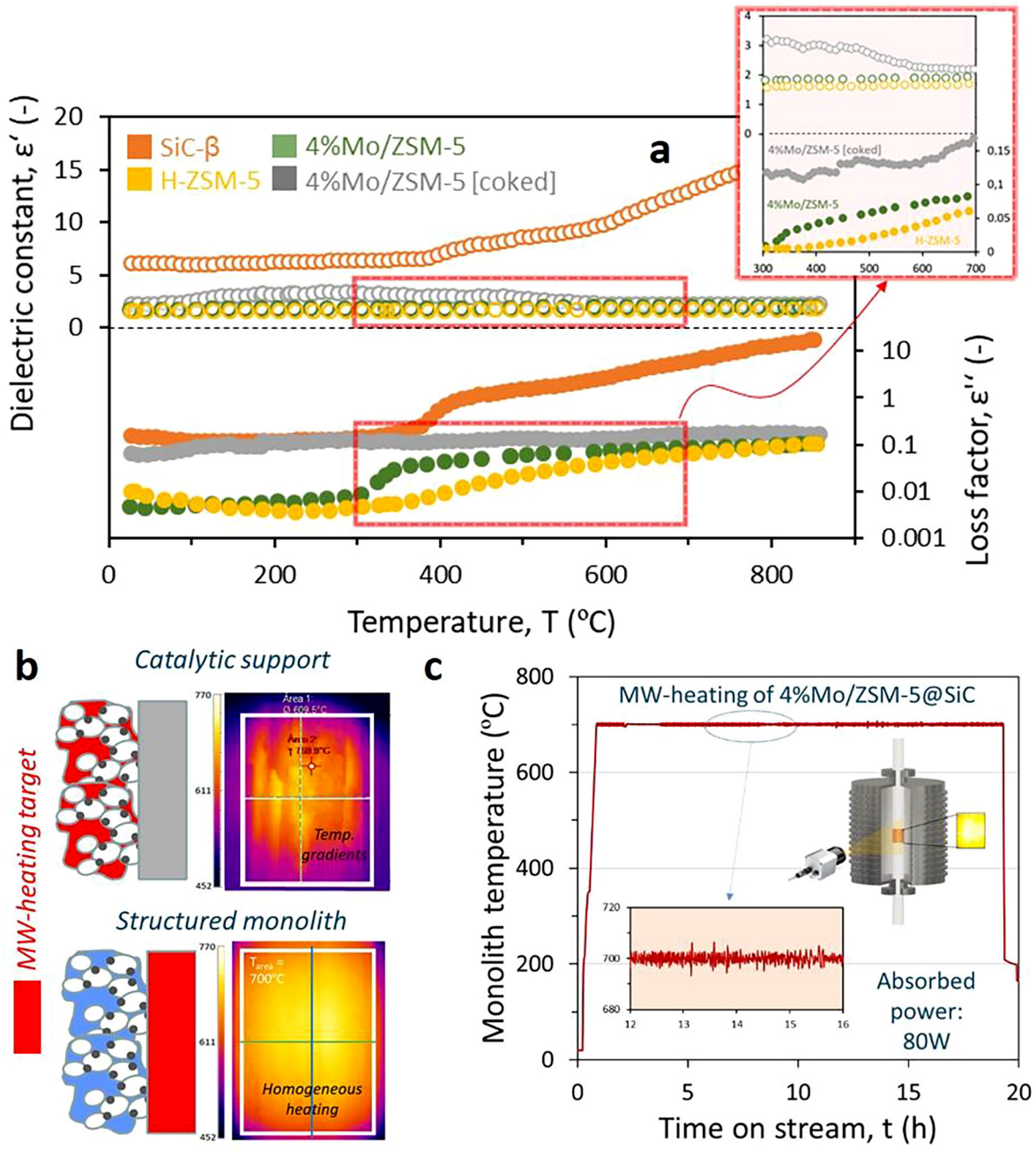

Fig. 5. a) Evolution of the dielectric constant ε' (open symbols) and dielectric loss (filled symbols) of □ SiC (brown), □ H-ZSM-5 (yellow), □ 4%Mo/ZSM-5 (green) and □ coked-4%Mo/ZSM-5 (grey) with temperature, b) MW-heating type as a function of the target material: catalyst support (Mo/ZSM-5@cordierite) or structured monolith (Mo/ZSM-5@SiC), c) 4%Mo/ZSM-5@SiC temperature control under MW-assisted heating at MNOC reaction conditions (3000 mL/g_{cat}·h, CH4:N_2 = 80:20).

quantitative SEM-EDX analysis of the catalytic powder resulted in a Mo content of 3.58 ± 0.78 wt% and a Si/Al ratio of 12.9 ± 1.6. The textural appearance of the coated catalyst and the fresh calcined Mo/ZSM-5 powder (Fig. 4.f) did not change significantly, as revealed by SEM.

3.2. Microwave heating of catalytic monoliths

The dielectric properties of the involved materials were evaluated in the range of temperatures from 25 to 800 °C at 2.45 GHz. Fig. 5.a illustrates the evolution of the dielectric constant ε' and loss factor ε" of SiC powder, H-ZSM-5 zeolite, fresh and coked Mo/ZSM-5. In the case of cordierite, due to the extremely low dielectric loss, $\varepsilon"_{cordierite}$ (25 °C) ≈ 10^{-4} did not allow to heat the material under MW irradiation and to measure its dielectric properties at the same time using the apparatus described in the experimental section. The cordierite could be considered as MW transparent material. On the other hand, SiC is well known as a very good microwave absorber, and its dielectric loss and loss tangent δ is by far the highest, tan $\delta_{700\,°C}$ = 0.46, compared to the other materials in Fig. 5.a. The dielectric properties of zeolites at high temperatures, depend mainly on the movements of the cations at different exchange positions [37]. The dipoles created inside the zeolite cages between the negatively charge framework and the mobile cations are responsible of the MW heating. The number and size of the mobile cations, determined by its charge and the Si/Al ratio of the zeolite, define the ability of zeolites to be heated by MWs. In our case, the HZSM-5 with a nominal Si/Al ratio of 11.5 presents a relatively low value of loss tangent $\delta_{700\,°C}$ = 3.9 10^{-2}. When the ion-exchanged

molybdate species are inside the framework, the dielectric losses slightly increase up to tan $\delta_{700\,^{\circ}C} = 4.3\ 10^{-2}$.

Considering the dielectric properties discussed above, the MW-heating target becomes different between the two catalytic monoliths. The Mo/ZSM-5@cordierite involves the preferential heating of the zeolite whereas the Mo/ZSM-5@SiC involves the heating of the SiC structured support (see Fig. 5.b). On this regard, the use of the cordierite-based samples requires homogeneous coating in order to get an even temperature distribution along the sample, as it was previously reported by our group [34]. Another important aspect is that the losses in the coked sample are higher than in the original zeolite $\delta_{700\,^{\circ}C} = 7.6\ 10^{-2}$. Carbon materials are good microwave absorbers due to the interactions of delocalized π-electrons with MWs, thus converting MW energy into heat [48]. This means that the dielectric properties of the catalyst will be affected not only by changes in temperature but also by the chemical reaction. Therefore, inhomogeneous coke deposition on the catalyst surface may lead to uneven heating and eventual hot spots formation. As a result, the accurate control of the temperature in the resonator became extremely challenging when the Mo/ZSM-5@cordierite monolith was heated by MWs. For this reason, this monolith was discarded for further reaction tests. In contrast, Fig. 5.b illustrates that the use of SiC-based samples provides a homogeneous temperature distribution. In fact, it was proven that catalyst coking did not impact the heating stability of Mo/ZSM-5@SiC. Fig. 5.c shows that this monolith could perform the MNOC catalytic reaction during 20 h on stream under MW-assisted heating without temperature decay or thermal runaway. This excellent stability test reveals the convenience of selecting a proper monolithic support with suitable dielectric properties for MW irradiation.

3.3. Temperature measurements in MW and CH structured reactors

Following the procedure described in Section 2.4, the gas temperature downstream was measured during both conventional and microwave-assisted heating. Fig. 6.a displays a sample cooling test right after switching off microwaves, with the thermocouple located in the central point of the monolith. In this cooling test the temperature was monitored by the three probes at a time, illustrating the perfect correlation among the thermocouple and contactless thermometers measurements. In Fig. 6.a). it could be also observed that at time zero, there is a temperature gap between the thermocouple (gas phase) and the temperature registered by the camera (surface of the monolith). This gap could be considered as a rough estimation of the temperature gradient, $\Delta T_{G\text{-}S} = T_{sample,7.5mm} - T_{gas,7.5mm} \approx 712\,^{\circ}C – 693\,^{\circ}C \approx 19\,^{\circ}C$, between gas and catalytic wall surface. This value is lower than the 50 °C that we previously reported [34], because the actual approach is not a real 'in situ' measurement, since there is a time delay after switching off MWs and introducing thermocouple. This experimental result illustrates one of the potential roles of microwave-assisted heating on gas-solid catalytic process: MW heating could reduce or inhibiting gas-phase reactions due to the temperature gradient between the catalytic surface and the bulk gas phase. This was recently corroborated in our group for the oxidative dehydrogenation of alkenes under MW irradiation [49].

Fig. 6.b) depicts the temperature measurements vs distance along the quartz tube, recorded under reaction conditions, for MW and CH. Under MW-heating it can be observed that, 2 mm away from the sample, the gas temperature is roughly 150 °C lower than that of the sample ($T_{gas,-2mm} = 544\,^{\circ}C$ vs $T_{sample,0mm} = 700\,^{\circ}C$). In contrast, the gases exiting the reactor heated in the conventional oven need around 40 mm to reach the same temperature.

3.4. MNOC reaction studies under conventional and microwave assisted heating

Prior to MNOC testing, a thorough calibration of reaction gases was performed as described in Section 2.3. The standard deviation of the peak areas detected for some relevant reaction gases at a given concentration are: $\sigma_{80\%CH4\text{-}TCD} = 0.03\%$, $\sigma_{20\%N2\text{-}TCD} = 0.12\%$, $\sigma_{15\%H2\text{-}TCD} = 0.12\%$, $\sigma_{2\%C2H4\text{-}FID} = 1.90\%$, $\sigma_{0.2\%C6H6\text{-}FID} = 0.95\%$, $\sigma_{0.1\%C7H8\text{-}FID} = 0.61\%$. The linearity between gas concentration and output signal was preserved for every species in a wide concentration range. As an example, the regression coefficient of the linear trend between CH_4 concentration and its output signal was $r^2 = 0.997$ along the range of evaluated concentrations: 0% - 85%. The response factors obtained along the calibration for the different species were employed for the analysis of the outlet reaction gases and, thus, support the CH_4 conversion and hydrocarbon selectivity results described below.

Initial experimental MNOC tests using the structured Mo/ZSM-5@SiC were conducted at high space velocity 6000 $mL/g_{cat}h$ in order to investigate primary reaction products [50]. The monolith was tested first under conventional heating, followed by regeneration to remove coke and after that it was heated by MWs. The same experiment was also conducted with a new sample in the reverse order and the observed conversion and product distribution was the same. The values of the methane conversion (Fig. 7) were similar around 10–11%, regardless the heating mechanism, since in both cases the temperature measured on the catalyst was 700 °C and temperature distribution, observed with the IR camera, was homogenous on the surface of the monolith.

However, the product distribution was very different depending on the heating mechanism (Figs. 7 and 8). First of all, the coke productivity, measured as the remaining amount of carbon to close the transient mass balance for C species, was significantly lower under MW heating: Y_C [MW] (200 min) = 2.20% wt.% than under conventional heating Y_C [CH] (200 min) = 5.49 wt%. On this regard, the solid-gas temperature gradient and the gas temperature profiles presented in Fig. 6.b suggest that the MNOC process may easily undergo polyaromatic hydrocarbons PAH and soft coke formation under conventional heating, whereas MW-heating would eventually inhibit these gas-phase reactions thanks to the induced gas-solid temperature gradient. This agrees with the fact that the production of polyaromatics is avoided using MW heating. As a consequence, the formation of amorphous coke must be somehow minimized. Concerning product distribution in both cases (CH and MWH) a sharp increase of CO concentration was observed, being more important in the case of MWH (Fig. 7). The carbon monoxide production is attributed to the carbothermal reduction of MoO_3 into Mo_2C [35,36]. The initial CH_4 reactions with the MoO_x species, well dispersed in the zeolitic pores, led first to the removal of oxygen as CO, CO_2, and H_2O and to the introduction of carbidic carbons into the reduced structures forming the Mo_2C, which is widely recognized as the active phase in the catalyst, and the initial stage in the MNOC mechanism [9,10,18]. In fact, either in CH or MWH after the CO sharp increase, the benzene product starts to appear. However in the case of MWH this is accompanied by the production of C_2H_2, a reaction product that was rarely reported for this reaction [28,50,51]. The formation of acetylene has been also recently reported in the reaction of methane with iron carbide cluster anions under high temperature conditions [52]. In the case of methane dehydroaromatization (MDA), Meriaudeau et al. [50] observed that the acetylene pressure increases when contact time decreases while the opposite is observed for ethylene and benzene. This observation suggested that acetylene could be the primary product whereas C_2H_4 and C_6H_6 exhibit the behaviour of secondary products, with respect to the contact time. These authors proposed a monofunctional mechanism for the MDA where only the Mo_2C species are the active phase, not only responsible for the activation of the C—H bond (to obtain the intermediate acetylene and ethylene) but also for the aromatization into benzene which, according to them, occurs exclusively over Mo carbide species. The hypothesis of the monofunctional mechanism was also recently supported by Kosinov et al. [15] who prepared very well dispersed precursor MoO_x species on the channels of ZSM-5 and silicalite. These authors demonstrated that the formation of benzene was possible in the case of silicalite. However,

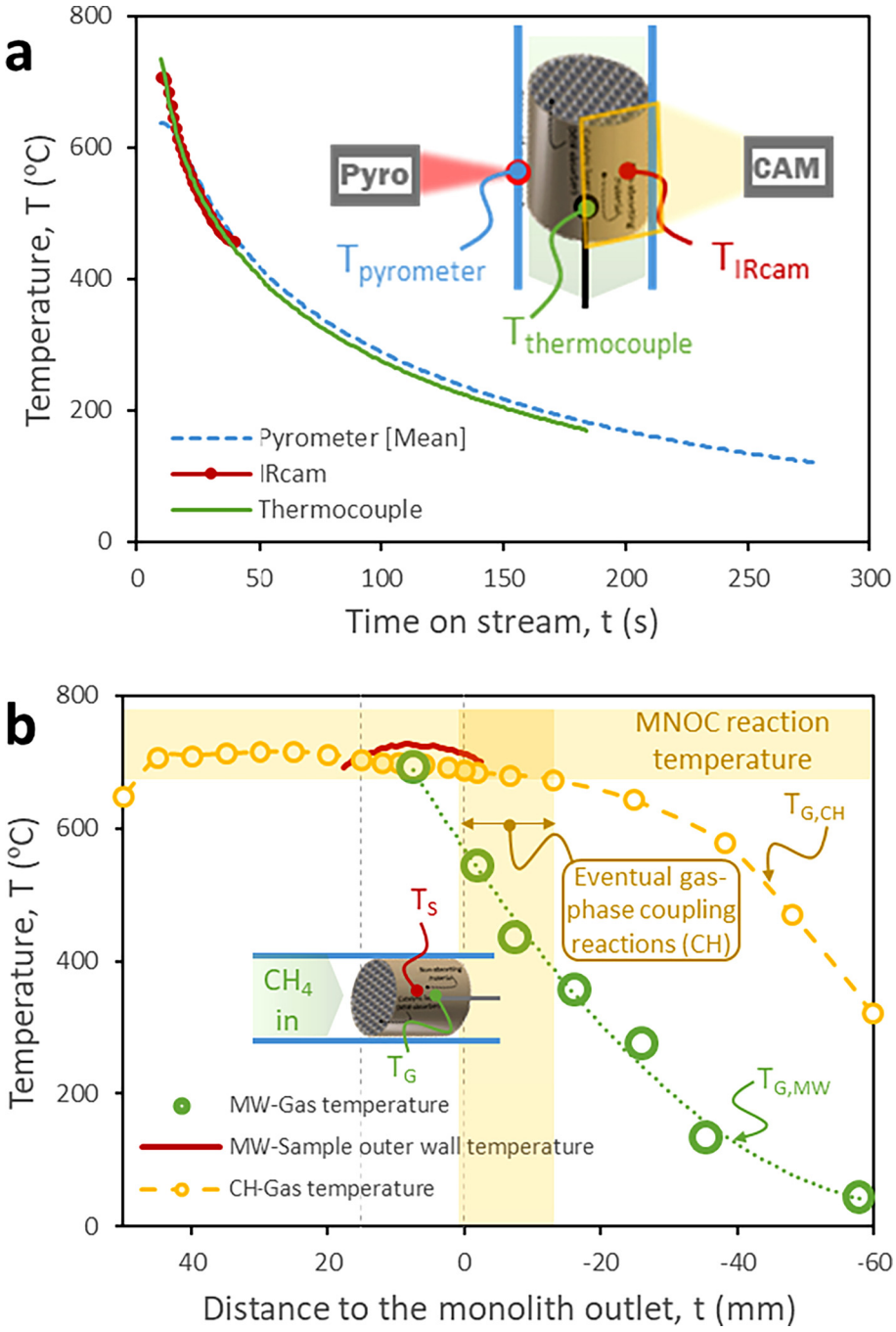

Fig. 6. a) Comparison of temperature values measured by thermocouple, infrared camera and pyrometer during system cooling down, b) Axial catalyst and gas-phase temperature profiles during MNOC operation under conventional (CH) and microwave-assisted heating (MW).

a faster deactivation and lower selectivity was obtained, indicating that the distribution of the Mo_2C species is different in both zeolites. Nevertheless, these hypotheses contrast with the bifunctional mechanism suggested by several authors proposing that the cyclization of the intermediates takes place in the Brönsted acid sites of the zeolite [16,19,53]. This mechanism, introduced for the first time by Wang et al. (1993) [54], has been mostly accepted in the recent years [55].

In our case, the hypothesis is that the nature of the Mo_2C species formed along the activation period, responsible of the activity and selectivity in MDA, becomes different than that under conventional heating due to the selective heating of the MoO_x species using microwave radiation. The selective and fast heating could eventually lead to the formation of isolated Mo_2C clusters on the channels of the zeolite. Although we could not demonstrate it experimentally, the previous speculation is supported by the evolution of the different reaction products during the initial formation of the molybdenum carbide species. Fig. 8 shows the hydrocarbon selectivities, calculated without accounting for the coke formation, and methane conversion for MNOC under conventional and MW-assisted heating at different reaction times (100 min and 200 min). The presence of heavy aromatics, the main precursors for coke formation, is strongly reduced under MW heating conditions in comparison with conventional heating (Fig. 8). The methyl radical formed on Mo_2C active sites, after consecutive reaction steps, ends up into light hydrocarbon molecules and, mainly, benzene and naphthalene thanks to the shape-selectivity of the employed zeolites and zeotypes (essentially, ZSM-5 and MCM-22). Apart from these

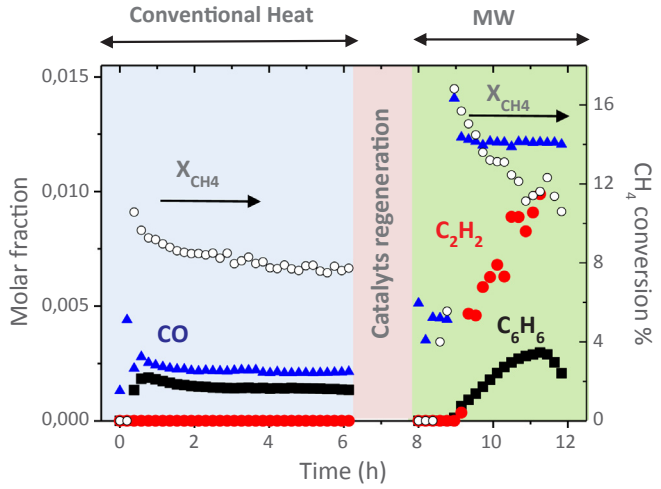

Fig. 7. Evolution of molar fraction of CO, C_2H_2 and C_6H_6 and CH_4 conversion under conventional and microwave heating. 4%Mo/ZSM-5@SiC operating at 700 °C and 6000 mL/g_{cat}h under conventional (light blue background) and microwave-assisted heating (light green).

hydrocarbons, side reactions over the acidic surface of the catalyst and in the gas phase lead to the formation of coke deposits of different nature. In the case of the gas-phase, the formation of highly dehydrogenated polyaromatic hydrocarbon (PAH) compounds derived from benzene and naphthalene molecules occurs at reaction temperatures higher than 680 °C. According to this hypothesis, the low gas-phase temperature in the MW-assisted process would prevent some coke forming reactions to occur.

This finding opens news possibilities in the field of methane valorization via catalytic MNOC, heated by MWs. Firstly, MW heating influences the distribution and the formation of Mo_2C species compared to CH resulting in more selective species at the initial stage. Moreover, MW-heating appears here as promising tool to identify reaction intermediates and to gain insight into the complex methane dehydrogenation reaction mechanism. Taking advantage of the fast heating capabilities of the MW sources and the temperature gradient between the catalyst surface and the surrounding fluid, microwave radiation could be potentially employed to activate and/or stop the methane coupling reaction mechanism on demand, thus, gaining insight into the nature of the intermediate species. Secondly, this gas-solid temperature gradient reduces the soft coke formation via PAH production along the aromatization process in the MNOC reaction. The proposed MW heated reactor system seems to inhibit this soft coke contribution to some extent, thus, limiting the activity decay for more extended periods of reactions. To illustrate that, Fig. 9 shows the MNOC performance on Mo/ZSM-5@SiC at the spatial velocity of 3000 mL/g_{cat}h. In terms of methane conversion and hydrocarbon yield, a very low deactivation is observed after 4 h on stream, working in a stable regime for at least eight additional hours. The confirmation of the previous hypothesis on the gas-solid temperature gradient and its impact on the catalytic process selectivity may open a new paradigm for deactivation strategies based on the improved system stability offered by MW-assisted heating systems.

With respect to the results available in literature for the non-oxidative coupling of methane in the last decade [10,13], both the methane conversion and conversion decay reported in this work are very similar to those highlighted in the recent review by Sun et al. [10], i.e. initial CH_4 conversion around 15% and conversion decay approximately down to 10% along 12 h on stream. It must be pointed out that the spatial velocity employed in Fig. 9 is twice as high as that used in literature (working with fixed beds of Mo/ZSM-5 powder heated under conventional heating). On the contrary, hydrocarbon yields are different. In literature, aromatic yields typically raise up to 8% at the beginning of the experiment (usually, $Y_{C6H6} \approx 6\%$ and $Y_{C10H8} \approx 2\%$) and remain around 6% after some hours on stream. The overall hydrocarbon yield decay due to soft coking in this work was, thus, comparable to that reported in the literature in spite of using more severe conditions, i.e. twice higher methane throughputs.

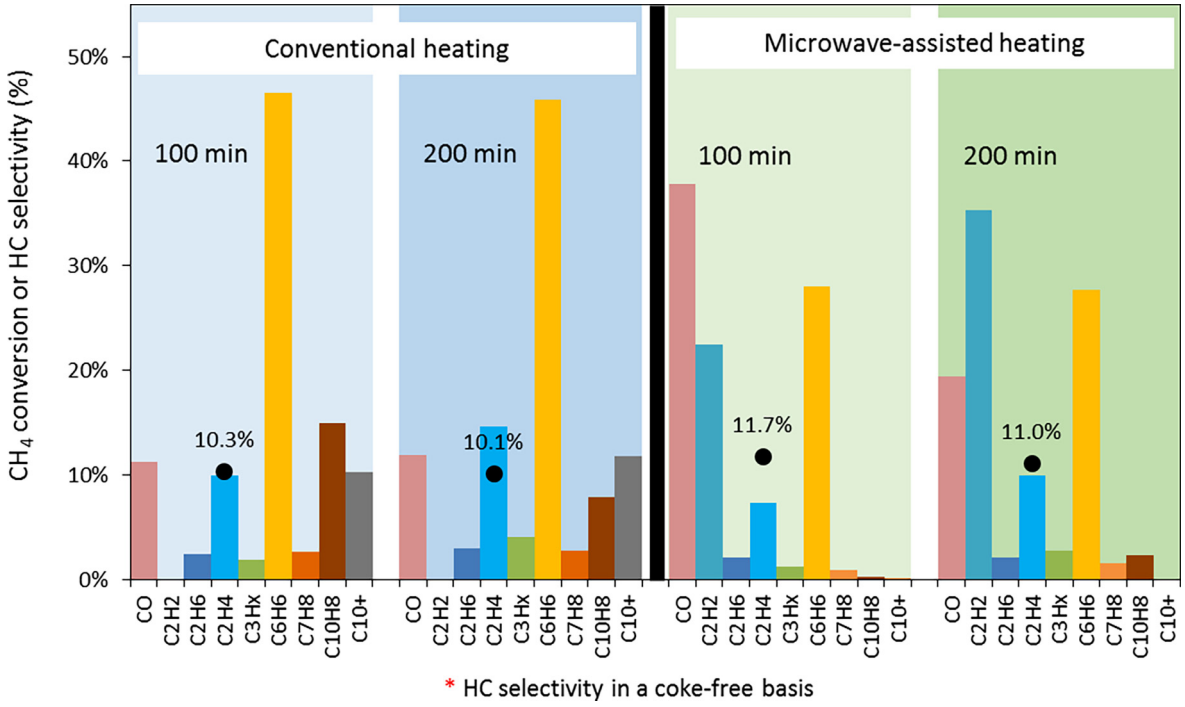

Fig. 8. Methane conversion and hydrocarbon products selectivity (coke-free basis) after 100 min and 200 min on stream for MNOC on 4%Mo/ZSM-5@SiC operating at 700 °C and 6000 mL/g_{cat}h, being CH_4:N_2 = 75:25 under conventional (light blue background) and microwave-assisted heating (light green).

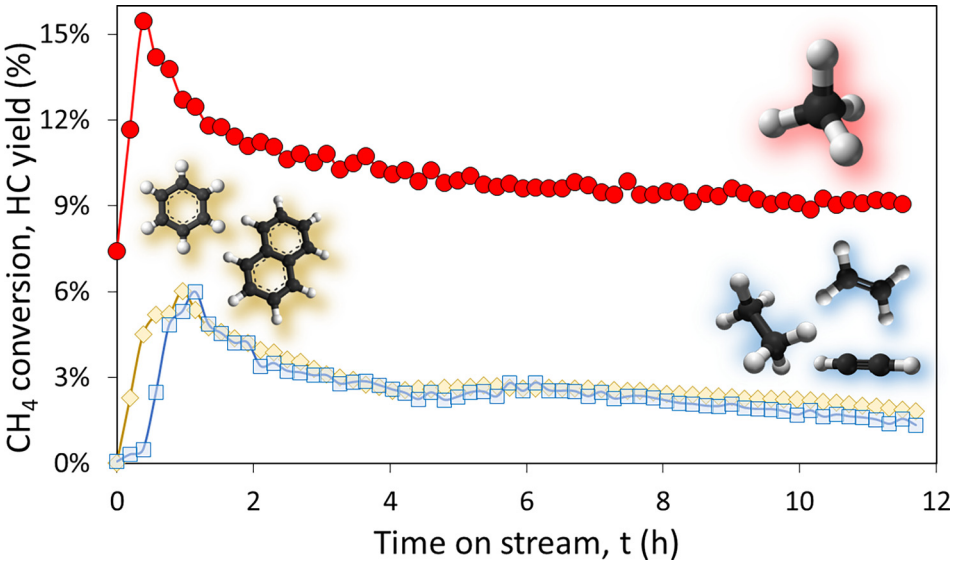

Fig. 9. Transient methane conversion and hydrocarbon yield for MNOC reaction under MW-heating. Operational conditions: 4% Mo/ZSM-5@SiC (700 °C, 3000 mL/g_{cat}h, CH_4:N_2 = 80:20). ○ Methane conversion [circle], □ C_2 yield (ethane + ethylene + acetylene) [square], ◊ C_{6+} yield (benzene + naphthalene) [diamond].

4. Conclusions

A robust and stable microwave heated system has been developed. It consists of a SiC structured reactor coated with Mo-ZSM5 catalyst, heated in a cylindrical microwave cavity. We have demonstrated that the temperature control of the catalytic monolith under MW-heating is possible despite the change of its dielectric properties due to eventual coking. The temperature distribution on the surface of the monolith was measured under MW heating with a thermographic camera and it was homogeneous and stable for at least 19 h under reaction conditions. The catalytic activity of the Mo-ZSM5@SiC structured was evaluated under MW and conventional heating at the same temperature, 700 °C, resulting in similar conversion but totally different product distribution. The production of coke under conventional heating doubles the amount observed under MW heating. The product distribution in MWs was shifted towards C_2 hydrocarbons and C_6H_6 without formation of PAH and negligible amounts of naphthalene. In contrast, these heavy aromatic products, precursors of coke, are observed under CH. We hypothesize that the selective microwave heating may have an effect in the formation of the active catalytic species of Mo_2C inside the microporous support, affecting the selectivity and product distribution. This is supported by the different evolution of product distribution at the initial stages of the reaction. Furthermore, the gas-solid temperature gradient would prevent the formation of coke from PAHs in the gas phase. These two unique effects come solely from heating with microwave and cannot be observed when conventional heating mechanisms operate in the reactor. These results open up new possibilities for process intensification using alternative sources of energy as is the case of microwaves, for heating structured catalytic reactors.

Acknowledgements

Financial support from the European Union's Horizon 2020 Research and Innovation Programme (ADREM project – Grant Agreement No. 680777) is gratefully acknowledged. The microscopy measurements were conducted at the Laboratorio de Microscopias Avanzadas, Instituto de Nanociencia de Aragon, Universidad de Zaragoza, Spain. The synthesis of materials has been performed by the Platform of Production of Biomaterials and Nanoparticles of the NANOBIOSIS ICTS, more specifically by the Nanoparticle Synthesis Unit of the CIBER in BioEngineering, Biomaterials & Nanomedicine (CIBER-BBN).

References

[1] BP, BP Statistical Review of World Energy 2017 (2016).
[2] R. Horn, R. Schloegl, Methane activation by heterogeneous catalysis, Catal. Lett. 145 (2015) 23–39.
[3] Z.R. Ismagilov, E.V. Matus, L.T. Tsikoza, Direct conversion of methane on Mo/ZSM-5 catalysts to produce benzene and hydrogen: achievements and perspectives, Energ. Environ. Sci. 1 (2008) 526–541.
[4] D. Wang, J.H. Lunsford, M.P. Rosynek, Characterization of a Mo/ZSM-5 catalyst for the conversion of methane to benzene, J. Catal. 169 (1997) 347–358.
[5] Y. Shu, D. Ma, L. Xu, Y. Xu, X. Bao, Methane dehydro-aromatization over Mo/MCM-22 catalysts: a highly selective catalyst for the formation of benzene, Catal. Lett. 70 (2000) 67–73.
[6] K. Gao, J. Yang, A. Seidel-Morgenstern, C. Hamel, Methane dehydro-aromatization: potential of a Mo/MCM-22 catalyst and hydrogene-selective membranes, Chem. Ing. Tech. 88 (2016) 168–176.
[7] C.H.L. Tempelman, M. Teresa Portilla, M.E. Martinez-Armero, B. Mezari, N.G.R. de Caluwe, C. Martinez, E.J.M. Hensen, One-pot synthesis of nano-crystalline MCM-22, Micro, Meso. Mat. 220 (2016) 28–38.
[8] X. Yin, N. Chu, J. Yang, J. Wang, Z. Li, Synthesis of the nanosized MCM-22 zeolite and its catalytic performance in methane dehydro-aromatization reaction, Catal. Com. 43 (2014) 218–222.
[9] P. Schwach, X. Pan, X. Bao, Direct conversion of methane to value-added chemicals over heterogeneous catalysts: challenges and prospects, Chem. Rev. 117 (2017) 8497–8520.
[10] K. Sun, D.M. Ginosar, T. He, Y. Zhang, M. Fan, R. Chen, Progress in nonoxidative dehydroaromatization of methane in the last 6 years, Ind. Eng. Chem. Res. 57 (2018) 1768–1789.
[11] J.J. Spivey, G. Hutchings, Catalytic aromatization of methane, Chem. Soc. Rev. 43 (2014) 792–803.
[12] S. Majhi, P. Mohanty, H. Wang, K.K. Pant, Direct conversion of natural gas to higher hydrocarbons: a review, J. Energ. Chem. 22 (2013) 543–554.
[13] S. Ma, X. Guo, L. Zhao, S. Scott, X. Bao, Recent progress in methane dehydroaromatization: From laboratory curiosities to promising technology, J. Energ. Chem. 22 (2013) 1–20.
[14] W. Taifan, J. Baltrusaitis, CH4 conversion to value added products: Potential, limitations and extensions of a single step heterogeneous Catal, Appl. Catal. B: Environ. 198 (2016) 525–547.
[15] N. Kosinov, F.J.A.G. Coumans, E.A. Uslamin, A.S.G. Wijpkema, B. Mezari, E.J.M. Hensen, Methane Dehydroaromatization by Mo/HZSM-5: Mono- or Bifunctional Catal.? ACS Catal. 7 (2017) 520–529.
[16] C. Karakaya, H. Zhu, R.J. Kee, Kinetic modeling of methane dehydroaromatization chemistry on Mo/Zeolite catalysts in packed-bed reactors, Chem. Eng. Sci. 123 (2015) 474–486.
[17] Y. Song, Y. Xu, Y. Suzuki, H. Nakagome, X. Ma, Z. Zhang, The distribution of coke formed over a multilayer Mo/HZSM-5 fixed bed in H-2 co-fed methane aromatization at 1073 K: Exploration of the coking pathway, J. Catal. 330 (2015) 261–272.
[18] C. Karakaya, S.H. Morejudo, H. Zhu, R.J. Kee, Catalytic Chemistry for Methane Dehydroaromatization (MDA) on a Bifunctional Mo/HZSM-5 Catalyst in a Packed Bed, Ind. Eng. Chem. Res. 55 (2016) 9895–9906.
[19] K.S. Wong, J.W. Thybaut, E. Tangstad, M.W. Stocker, G.B. Marin, Methane aromatisation based upon elementary steps: kinetic and catalyst descriptors, Micro. Meso. Mat. 164 (2012) 302–312.
[20] M. Teresa Portilla, F.J. Llopis, C. Martinez, Non-oxidative dehydroaromatization of methane: an effective reaction-regeneration cyclic operation for catalyst life extension, Catal, Sci. Technol. 5 (2015) 3806–3821.

[21] J. Bai, S. Liu, S. Xie, L. Xu, L. Lin, Shape selectivity in methane dehydroaromatization over Mo/MCM-22 catalysts during a lifetime experiment, Catal. Lett. 90 (2003) 123–130.

[22] R. Borry, Y. Kim, A. Huffsmith, J. Reimer, E. Iglesia, Structure and density of Mo and acid sites in Mo-exchanged H-ZSM5 catalysts for nonoxidative methane conversion, J. Phys. Chem. B 103 (1999) 5787–5796.

[23] H. Liu, X. Bao, Y. Xu, Methane dehydroaromatization under nonoxidative conditions over Mo/HZSM-5 catalysts: Identification and preparation of the Mo active species, J. Catal. 239 (2006) 441–450.

[24] D. Ma, D. Wang, L. Su, Y. Shu, Y. Xu, X. Bao, Carbonaceous deposition on Mo/HMCM-22 catalysts for methane aromatization: a TP technique investigation, J. Catal. 208 (2002) 260–269.

[25] W. Ding, S. Li, G. Meitzner, E. Iglesia, Methane conversion to aromatics on Mo/H-ZSM5: structure of molybdenum species in working catalysts, J. Phys. Chem. B 105 (2001) 506–513.

[26] Y. Kim, R. Borry, E. Iglesia, Genesis of methane activation sites in Mo-exchanged H-ZSM-5 catalysts, Micro. Meso. Mat. 35–6 (2000) 495–509.

[27] C.H.L. Tempelman, E.J.M. Hensen, On the deactivation of Mo/HZSM-5 in the methane dehydroaromatization reaction, Appl. Catal. B-Environ. 176 (2015) 731–739.

[28] V. Ha, L. Tiep, P. Meriaudeau, C. Naccache, Aromatization of methane over zeolite supported molybdenum: active sites and reaction mechanism, J. Molec. Catal. A-Chem. 181 (2002) 283–290.

[29] I. Vollmer, G. Li, I. Yarulina, N. Kosinov, E.J. Hensen, K. Houben, D. Mance, M. Baldus, J. Gascon, F. Kapteijn, Relevance of the Mo-precursor state in H-ZSM-5 for methane dehydroaromatization, Catal. Sci. Technol. 8 (2018) 916–922.

[30] S. Mishra, S. Balyan, K.K. Pant, M.A. Haider, Non-oxidative conversion of methane into higher hydrocarbons over Mo/MCM-22 catalyst, J. Chem. Sci. 129 (2017) 1705–1711.

[31] A.I. Stankiewicz, J.A. Moulijn, Process intensification: Transforming chemical engineering, Chem. Eng. Prog. 96 (2000).

[32] B. Fidalgo, J.A. Menendez, Study of Energy consumption in a laboratory pilot plant for the microwave-assisted CO2 reforming of CH4, Fuel Proc. Technol. 95 (2012) 55–61.

[33] L.S. Gangurde, G.S.J. Sturm, M.J. Valero-Romero, R. Mallada, J. Santamaria, A.I. Stankiewicz, G.D. Stefanidis, Synthesis, characterization, and application of ruthenium-doped SrTiO3 perovskite catalysts for microwave-assisted methane dry reforming, Chem. Eng. Proc. 127 (2018) 178–190.

[34] A. Ramirez, J.L. Hueso, R. Mallada, J. Santamaria, In situ temperature measurements in microwave-heated gas-solid catalytic systems. Detection of hot spots and solid-fluid temperature gradients in the ethylene epoxidation reaction, Chem. Eng. J. 316 (2017) 50–60.

[35] T. Durka, T. Van Gerven, A. Stankiewicz, Microwaves in heterogeneous gas-phase catal.: experimental and numerical approaches, Chem. Eng. Technol. 32 (2009) 1301–1312.

[36] G.D. Stefanidis, A.N. Munoz, G.S.J. Sturm, A. Stankiewicz, A helicopter view of microwave application to chemical processes: reactions, separations, and equipment concepts, Rev. Chem. Eng. 30 (2014) 233–259.

[37] J. Gracia, M. Escuin, R. Mallada, N. Navascues, J. Santamaria, Heating of zeolites under microwave irradiation: a density functional theory approach to the ion movements responsible of the dielectric loss in Na, K, and Ca A-Zeolites, J. Phys. Chem. C 117 (2013) 15659–15666.

[38] J. Gracia, M. Escuin, R. Mallada, N. Navascues, J. Santamaria, Nano-heaters: new insights on the outstanding deposition of dielectric Energy on perovskite nanoparticles, Nano Energ. 20 (2016) 20–28.

[39] H. Nigar, B. Garcia-Banos, F.L. Penaranda-Foix, J.M. Catala-Civera, R. Mallada, J. Santamaria, Amine-functionalized mesoporous silica: a material capable of CO2 adsorption and fast regeneration by microwave heating, AIChE J. 62 (2016) 547–555.

[40] X. Zhang, D.O. Hayward, Applications of microwave dielectric heating in environment-related heterogeneous gas-phase catalytic systems, Inorg. Chim. Acta 359 (2006) 3421–3433.

[41] A. Eleta, P. Navarro, L. Costa, M. Montes, Deposition of zeolitic coatings onto Fecralloy microchannels: washcoating vs. in situ growing, Micro, Meso. Mat. 123 (2009) 113–122.

[42] J. Rouquerol, P. Llewellyn, F. Rouquerol, Is the BET equation applicable to microporous adsorbents), Stu. Surf. Sci. Catal. 160 (2006) 49–56.

[43] J.M. Catala-Civera, A.J. Canos, P. Plaza-Gonzalez, J.D. Gutierrez, B. Garcia-Banos, F.L. Penaranda-Foix, Dynamic measurement of dielectric properties of materials at high temperature during microwave heating in a dual mode cylindrical cavity, IEEE T. Microw. Theory 63 (2015) 2905–2914.

[44] C.A. Balanis, Antenna Theory: Analysis and Design, Wiley, 1982.

[45] W. Li, G. Meitzner, R. Borry, E. Iglesia, Raman and X-ray absorption studies of Mo species in Mo/H-ZSM5 catalysts for non-oxidative CH4 reactions, J. Catal. 191 (2000) 373–383.

[46] K. Chen, S. Xie, A. Bell, E. Iglesia, Structure and properties of oxidative dehydrogenation catalysts based on MoO3/Al2O3, J. Catal. 198 (2001) 232–242.

[47] A.F. Pérez-Cadenas, F. Kapteijn, J.A. Moulijn, Tuning the morphology of monolith coatings, Appl. Catal. A: Gen. 319 (2007) 267–271.

[48] J.A. Menendez, A. Arenillas, B. Fidalgo, Y. Fernandez, L. Zubizarreta, E.G. Calvo, J.M. Bermudez, Microwave heating processes involving carbon materials, Fuel Proc. Technol. 91 (2010) 1–8.

[49] A. Ramírez, Reactores catalíticos gas-sólido con calentamiento directo del sólido en campo microondas, PhD thesis (2017).

[50] P. Meriaudeau, L. Tiep, V. Ha, C. Naccache, G. Szabo, Aromatization of methane over Mo/H-ZSM-5 catalyst: on the possible reaction intermediates, J. Molec. Catal. A-Chem. 144 (1999) 469–471.

[51] C. Zhang, S. Li, Y. Yuan, W. Zhang, T. Wu, L. Lin, Aromatization of methane in the absence of oxygen over Mo-based catalysts supported on different types of zeolites, Catal. Lett. 56 (1998) 207–213.

[52] H. Li, L. Jiang, Y. Zhao, Q. Liu, T. Zhang, S. He, Formation of Acetylene in the Reaction of Methane with Iron Carbide Cluster Anions FeC3- under High-Temperature Conditions, Angew. Chem.-Int. Ed. 57 (2018) 2662–2666.

[53] M. Iliuta, I. Iliuta, B. Grandjean, F. Larachi, Kinetics of methane nonoxidative aromatization over Ru-Mo/HZSM-5 catalyst, Ind. Eng. Chem. Res. 42 (2003) 3203–3209.

[54] L. Wang, L. Tao, M. Xie, G. Xu, J. Huang, Y. Xu, Dehydrogenation and aromatization of methane under nonoxidizing conditions, Catal. Lett. 21 (1993) 35–41.

[55] I. Vollmer, I. Yarulina, F. Kapteijn, J. Gascón, Progress in developing a structure-activity relationship for the direct aromatization of methane, Chem. Cat. Chem. 10 (2018) 1–15.